Supporting Information

Exploiting Confinement to Study the Crystallization Pathway of Calcium Sulfate

Clara Anduix-Canto, Mark A. Levenstein, Yi-Yeoun Kim, Jose R. A. Godinho, Alexander N. Kulak, Carlos González Niño, Philip J. Withers, Jonathan P. Wright, Nikil Kapur, Hugo K. Christenson and Fiona C. Meldrum

Materials and Methods

Materials

$CaCl_2$ $2H_2O$, $(NH_4)_2SO_4$, succinic anhydride, toluene, (3-aminopropyl)triethoxysilane, 4-dimethyl(amino)pyridine, N,N-dimethylformamide, nitric acid and ethanol (>99.9 %) were purchased from Sigma-Aldrich and were used as received. Borosilicate glass capillaries with 1 mm outer diameters and 0.75 mm inner diameters were purchased from World Precision Instruments, Inc. The controlled pore glass (CPG) rods were obtained as Varapor100 from Advanced Glass and Ceramics (St. James, NC, USA) and had dimensions of 2.8 mm in diameter and 10 mm in length. They possess a narrow pore size distribution with mean pore size ≈ 7 nm, surface area 120 ± 10 m^2/g and porosity of 25 ± 4 % (Figure S1). The CPGs were cleaned by immersing the rods in 20% nitric acid at 100 °C for 2 h, washing with Milli-Q DI water (Millipore, 18.2 MΩ·cm) followed by ethanol, and then incubating in ethanol overnight before drying in the oven at 60°C for 3 h. All glassware including glass tubes and capillaries were cleaned overnight in "piranha solution" (30% H_2O_2 and 70% H_2SO_4), and were then rinsed with, and stored under DI water until required.

Crystallization in Controlled Pore Glass (CPG) Rods

The CPG rods were first filled with Milli-Q DI water by immersing them in water for at least 4h. Calcium sulfate was then precipitated within the rods by inserting their ends into pieces of

plastic tubing, which were in turn inserted into glass tubes. 3M $CaCl_2$ and $(NH_4)_2SO_4$ solutions were injected into these glass tubes, which were sealed. The plastic tubing and glass tubes were sealed with 6 mm His-3 Bag (3:1 ratio) shrink wrap (Figure S2).

Functionalization of the Surfaces of the CPGs

CPG rods were functionalized with carboxyl-terminated self-assembled monolayers (SAMs) by vapor silane deposition[1] of an amino-terminated silane followed by chemical conversion of the amino group to a carboxyl group. The CPG rods were first dried by immersing them in ethanol overnight, and then drying them at 60 °C for 3 h. They were then placed in a vacuum chamber with 1 mL of (3-aminopropyl)triethoxysilane for 1 h at room temperature. The silane was subsequently removed from the chamber and the CPG rods were kept under vacuum for 1 h at 45 °C to evaporate any remaining silane. The rods were then washed with toluene and ethanol and dried in an oven at 60 °C for 2 h. The amino-terminated SAMs were converted to carboxyl groups following standard methods.[2] The rods were immersed in a solution of 10% succinic anhydride and 1% 4-dimethyl(amino)pyridine in N,N-dimethylformamide (DMF) overnight, after which time they were washed with DMF, water and ethanol and dried in an oven at 60 °C for 2 h. Successful coating was confirmed by IR spectroscopy (Figure S1D).

Bulk Crystallization of Calcium Sulfate in Glass Capillaries

All bulk crystallization experiments were carried out under ambient conditions which, unless otherwise stated, corresponds to T = 20 ± 2 °C and relative humidity (r.h.) 40 ± 5 %. Control experiments were carried out by precipitating crystals within a 1 mm (internal diameter) glass capillary. A capillary filled with water was inserted between two plastic tubes, and 3M $CaCl_2$ and $(NH_4)_2SO_4$ solutions were then injected into the tubes.

In-situ Synchrotron X-ray Diffraction (XRD), Micro-Computed Tomography (μ-CT) and Diffraction Computed Tomography (XRDCT)

Combined synchrotron μ-CT and XRDCT[3, 4] were used to observe the formation of the different calcium sulfate phases. Experiments were conducted at ID11 (Materials Science beamline) at the European Synchrotron Radiation Facility (ESRF) Grenoble, France. Alternate diffraction and imaging scans were recorded. CPG rods were inserted into glass tubes as described previously and the seal closing the $CaCl_2$ reservoir was glued to an M4 screw attached to a rotating stage. The system was mounted vertically on the rotating stage with the $(NH_4)_2SO_4$ reservoir at the top.

XRDCT was performed by recording 2D X-ray diffraction (XRD) patterns at different z heights along the CPG rods, and these data were used to generate spatial diffraction maps of individual cross-sectional slices. XRDCT data were collected at 86 positions across the width of the 2.8 mm CPG rods with a 50 × 50 μm^2 beam of 40 keV (wavelength = 0.30996 Å) unless otherwise stated. Measurements were recorded with precise control over the translational (y-direction perpendicular to the incident beam) and rotational (ω-swing along vertical z-axis) steps, where XRD patterns were collected every 37.5 μm along the y-axis, and from 0 – 180° and then back from 180° to 0° for the next y step in 5° rotational steps (ω), with 1 sec exposure times.

2D XRD patterns were also recorded of large volumes of individual samples using a 0.4 × 0.4 mm^2 beam at 40 keV and exposure times of 1 sec. This yielded average data of the crystal phases present within a 0.16 mm^2 area at the centre of the rod. A 2D CCD area detector (FReLon 4M) coupled with a fibre optic taper was used for rapid readout of diffraction data. 1D diffraction profiles were obtained by azimuthal integration of 2D diffraction patterns using the pyFAI library with the iPython command shell. A CeO_2 standard was used to calibrate the beam centre and tilting relative to the Debye-Scherrer rings. A diffraction pattern of a rod filled

with water was used to subtract the glass background from the diffraction patterns of the CPG/ calcium sulfate samples.

The crystals within the 2.8 mm CPG rods were also imaged using μ-CT at beamline I13-2 at Diamond Light Source, where 3D tomograms were computationally reconstructed from the projection images. The images were collected with a high resolution pco edge 5.5 camera with a 2560 × 2160 pixel array and an effective pixel size of 1.6 μm. A total of 2000 projections were acquired per scan over 180°, with a field of view of 4.2 × 3.5 mm^2 and 0.1 sec exposure time.

Reconstruction of Tomography Data

The 2D diffraction patterns obtained at different spatial and angular positions were integrated to obtain 1D patterns as a function of 2θ. Integration, diffraction and tomographic reconstructions, data fitting and plotting were carried out using the iPython command shell. Spatial 2D diffraction maps were obtained by projection tomography, using an inversion in the Radon transform. The maps were obtained by selecting regions of interest in the diffraction patterns, where specific reflections for bassanite (110) and for gypsum (020) were employed. The intensities recorded are not absolute, such that direct comparison of the amounts of material present in different samples is not possible.

The reconstructed 16-bit μ-CT data from I13-2 was segmented using Avizo 9 and ImageJ. The analysis was carried out on resampled datasets with a 2 μm voxel size. A non-local means filter with parameters 10, 3 and 0.7 was applied to the tomograms to reduce the level of noise in the images. 3D images of the crystals in the rods were created in Avizo by rendering the tomograms based on their different intensity values.

Additional Characterization Methods

The surface areas, pore sizes and porosities of the CPG rods were determined using Barrett-Joyner-Halenda (BJH) and Brunauer–Emmett–Teller (BET) surface area analysis with nitrogen gas after degassing for 3 h at 120 °C using an ASAP 2020 (Accelerated Surface Area and Porosimetry System, Micrometrics). Crystals precipitated in glass capillaries and within the CPG rods were characterized *in situ* using a Nikon eclipse LV100 optical microscope. The different mineral phases were identified using a Renishaw 2000 Raman microscope equipped with a 785 nm diode laser. Raman spectra of crystals growing inside the CPG rods were collected *in situ* from intact rods. The laser was focused on different positions within the rod, where crystals were observed.

Transmission Electron Microscopy (TEM) and Scanning Transmission Electron Microscopy (STEM) were used to image cross-sections of CPG rods. Cross sections were prepared using Focused Ion beam (FIB) milling. The FIB milling was performed using FEI Helio G4 CX DualBeam-high resolution monochromated FEG-SEM with a precise Focused Ion Beam, equipped with Ga-beam and a field emission electron gun. The Ga ion beam was operated at 30 kV and at beam currents between 0.1 and 5 nA, and lift-out was performed *in situ* using a Kleindiek micromanipulator to transfer thin sections onto a copper TEM grid.

The internal structures of CPG rods containing calcium sulfate were investigated by TEM and STEM. The thin sections prepared by FIB milling were analyzed using an FEI Tecnai TF20 microscope fitted with a High-angle annular dark-field (HAADF) detector, INCA 350 Energy Dispersive X-ray (EDX) system/80 mm X-Max SDD detector and Gatan Orius SC600A CCD camera. Bright field TEM imaging and selected-area electron diffraction (SAED, 0.5 µm aperture) was conducted at 200 keV. The presence of crystals within the nanoporous CPG matrix were further confirmed using the HAADF-STEM dark field imaging mode, and EDX

elemental mapping of Ca, S and Si (Figure S11). The collection angle of the HAADF-STEM imaging was 80-240 mrad.

Simulations of Ion Diffusion through the CPG Rods

In order to estimate the ion concentration at any position along the rods over time before crystallization, the diffusion rate of the ions through the porous network was modelled using computer simulations. The concentration gradient of the ions in the pores is dependent on the porosity, pore geometry (tortuosity) and dimensions of the rod. This model permitted us to estimate the supersaturation at which nucleation occurs in the pores, assuming that no evaporation occurs and that the rod acts as a sealed system.

As the rods contain open pores, some evaporation inevitably occurs. Evaporation will promote crystallization on the surface of the rods, generating a flow of ions from the pores to the surface and therefore a concentration gradient from the core of the rod to its surfaces.[5] This velocity field within the rod will cause a competition between diffusion and advection effects. Our model is valid if diffusion effects dominate, but not if advection is the dominant force. This competition can be estimated by the Péclet number,

$$Pe = \frac{uL}{\varepsilon D_S^*} \qquad \text{Equation 1}$$

where L is the length of the porous rod (10 mm), D_S^* is the effective diffusion coefficient of the ions through the pores, ε is the porosity of the rod (0.25) and u is the velocity of the salt solution in the porous medium.[6] The velocity is related to the evaporation rate according to the following equation:

$$u = \frac{J}{A\rho} \qquad \text{Equation 2}$$

where J is the evaporation rate, A is the exposed surface area and ρ is the density of the liquid. J was calculated by weighing a dry CPG rod, then weighing the rod after immersing it in water

for 4h and calculating the time for the rod to completely dry, i.e. reach the initial weigh of the dry rod. The calculated *J* value for CPG rods of 2.8 mm in diameter was of $1 \cdot 10^{-6} g/s$. The effective diffusion coefficient of the ions in the pores is:

$$D_s^* = \frac{\varepsilon}{\tau} \cdot D_s \qquad \text{Equation 3}$$

where (τ) is the tortuosity, which is the degree of curvature or 'tortuousness' of a porous medium. The tortuosity of the system presented here is calculated with the equation $\tau = \varepsilon^{-0.25}$, where the internal structure is assumed to be a three-dimensional network of overlapping spheres.[7] Thus, the Péclet numbers were calculated using the parameters $\tau = 1.4$, $D_{Ca}^* = 1.25 \cdot 10^{-6}\ cm^2/s$ and $D_{So4}^* = 1.79 \cdot 10^{-6}\ cm^2/s$. According to Huinink *et al.*,[6] convection will dominate over diffusion at Pe > 1, when the ions are highly attracted to the surfaces of the system. For rods of 2.8 mm diameter 2.8 mm, Pe (Ca) = 0.8 and Pe (SO_4) = 0.5. As Pe < 1, we can consider evaporation through the open pores negligible.

Once the validity of the model was verified for CPG rods of 2.8 mm, the ion diffusion through the pores was simulated, and the concentration gradient of ions through the rods were plotted over time (Figure 1). From the ion concentration at the center of the rod it is then possible to calculate the supersaturation of the solution in the pores at a given time. Thus, the system was seen to reach supersaturation with respect to gypsum in around 40 min after 3 M reagent injection. Supersaturations were calculated with values of ion activity using Visual Minteq.

References

[1] S. Le Caer, F. Brunet, C. Chatelain, D. Durand, V. Dauvois, T. Charpentier, J. Ph. Renault, *J. Phys. Chem. C* **2012**, *116*, 4748.
[2] D. Archibald, S. Qadri, B. Gaber, *Langmuir* **1996**, *12*, 538.
[3] G. Harding, J. Kosanetzky, U. Neitzel, *Med. Phys.* **1987**, *14*, 515.
[4] P. Bleuet, E. Welcomme, E. Dooryhee, J. Susini, J. L. Hodeau, P. Walter, *Nat. Mater.* **2008**, *7*, 468.
[5] S. Veran-Tissoires, M. Marcoux, M. Prat, *EPL (Europhysics Letters)* **2012**, *98*, 34005.
[6] H. P. Huinink, L. Pel, M. A. J. Michels, *Phys. Fluids* **2002**, *14*, 1389.
[7] M. Matyka, Z. Koza, K. Vafai, *AIP Conf. Proc.* **2012**, *1453*, 17.

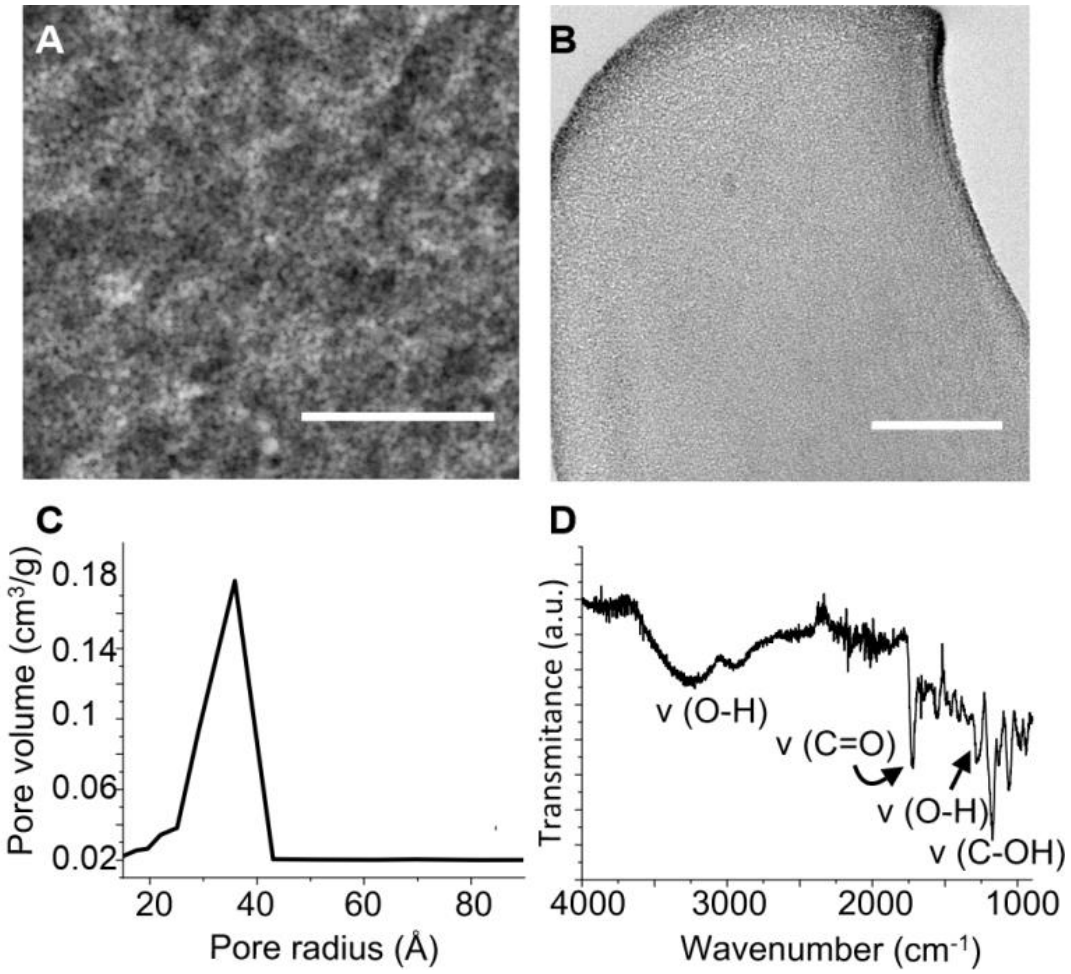

Figure S1. (A) SEM and (B) TEM images of the internal structure of a CPG rod. (C) BJH analysis shows that the pores are 7 nm in diameter. (D) FTIR spectrum of a carboxyl-functionalized CPG rod. Scale bars are 500 nm (A) and 50 nm (B).

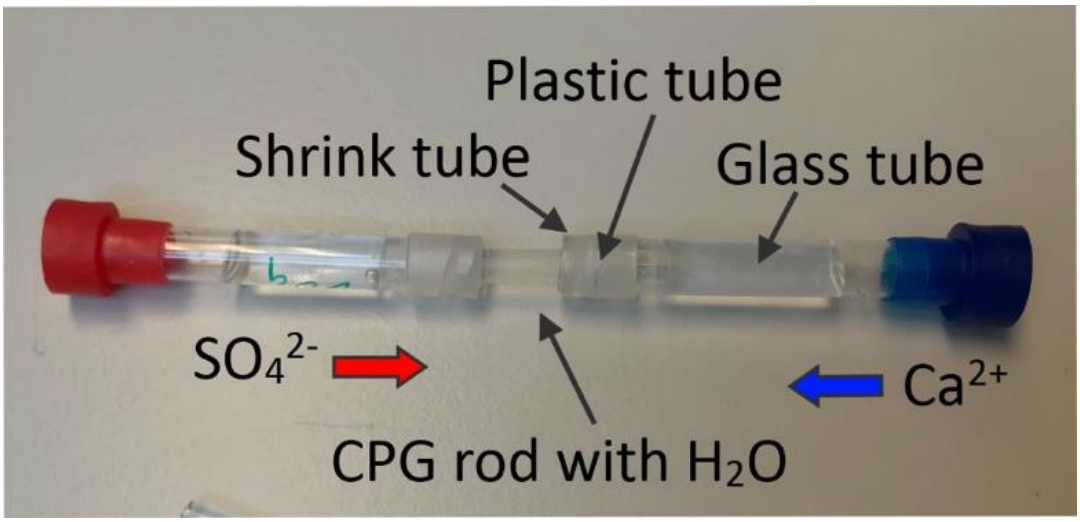

Figure S2. Set-up used for calcium sulfate precipitation in CPG rods. The rod filled with water is placed in between two tubes containing the reagent solutions that will diffuse through the pores.

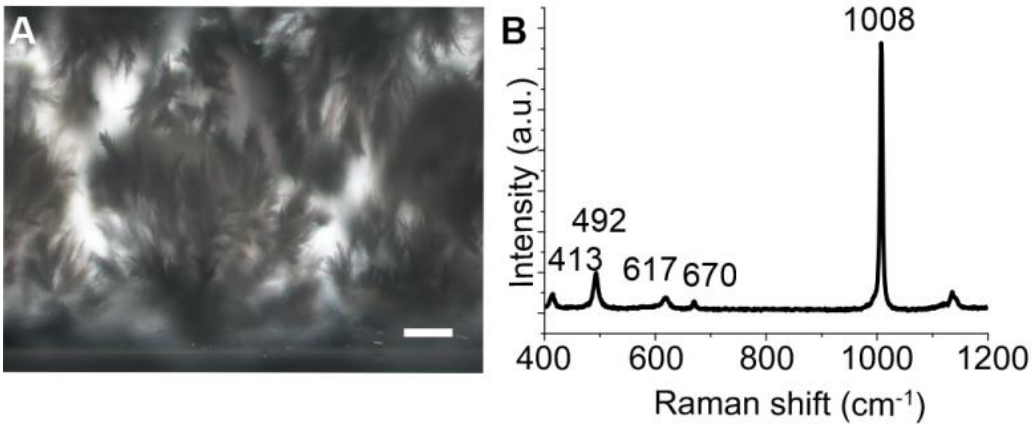

Figure S3. Optical micrograph (A) and Raman spectrum (B) of gypsum crystals precipitated within a 1 mm glass capillary 2 min after injecting equal volumes of 3M $CaCl_2$ and 3M $(NH_4)_2SO_4$ solutions from each end of the capillary. Scale bar is 100 μm.

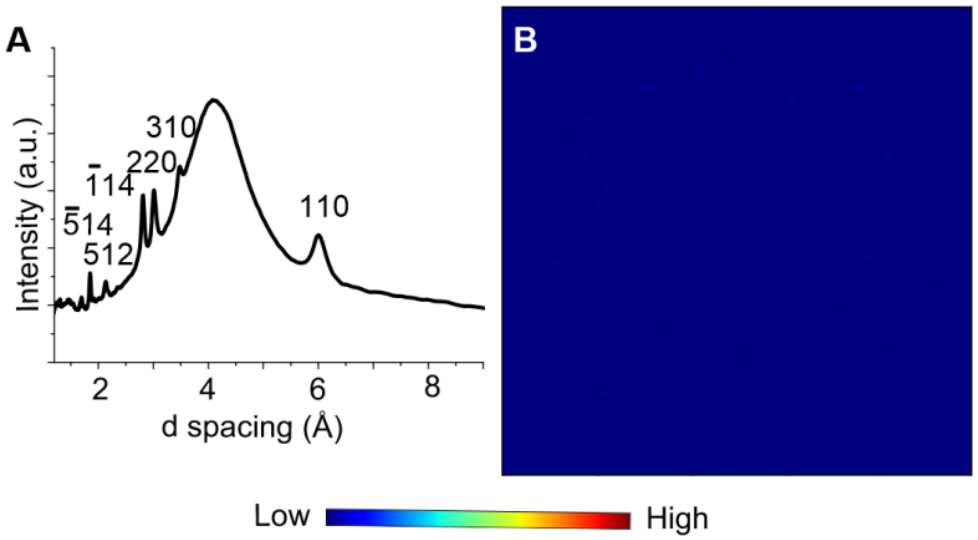

Figure S4. (A) X-ray diffraction pattern of bassanite crystals in a CPG rod after 24h. (B) 2D spatial diffraction map of crystals in the rod after 24h where the (020) reflection of gypsum was plotted, showing that no gypsum was present.

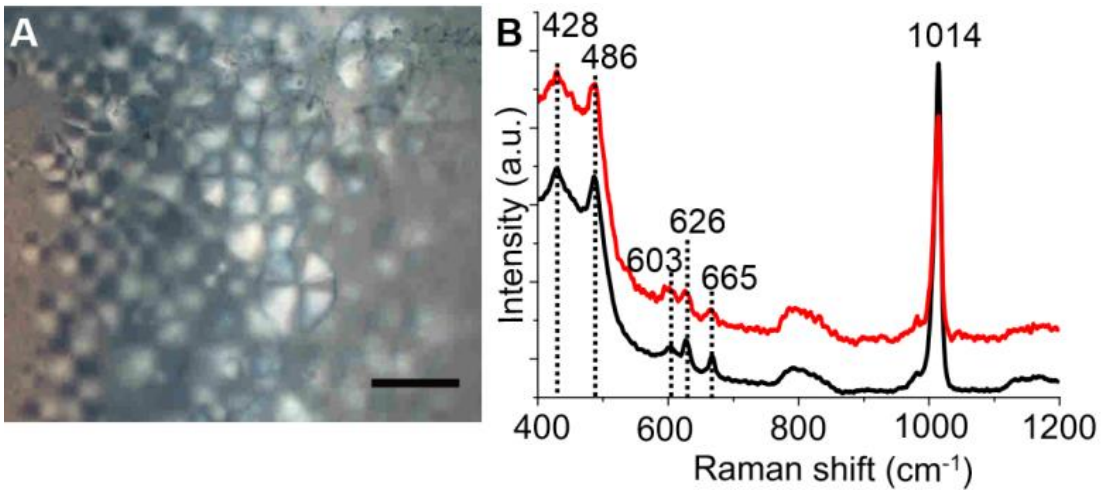

Figure S5. (A) Optical micrograph of calcium sulfate crystals growing inside a 7 nm porous rod under polarised light. (B) Raman spectrum of the crystals in the pores after 4 h (in black) and 3 weeks (in red) showing characteristic peaks from bassanite at 428 and 486 cm^{-1} $\nu_2(SO_4)$ (bending), 626 and 665 cm^{-1} $\nu_3(SO_4)$ and 1014 cm^{-1} $\nu_1(SO_4)$ (symmetric stretching). Scale bar is 100 μm.

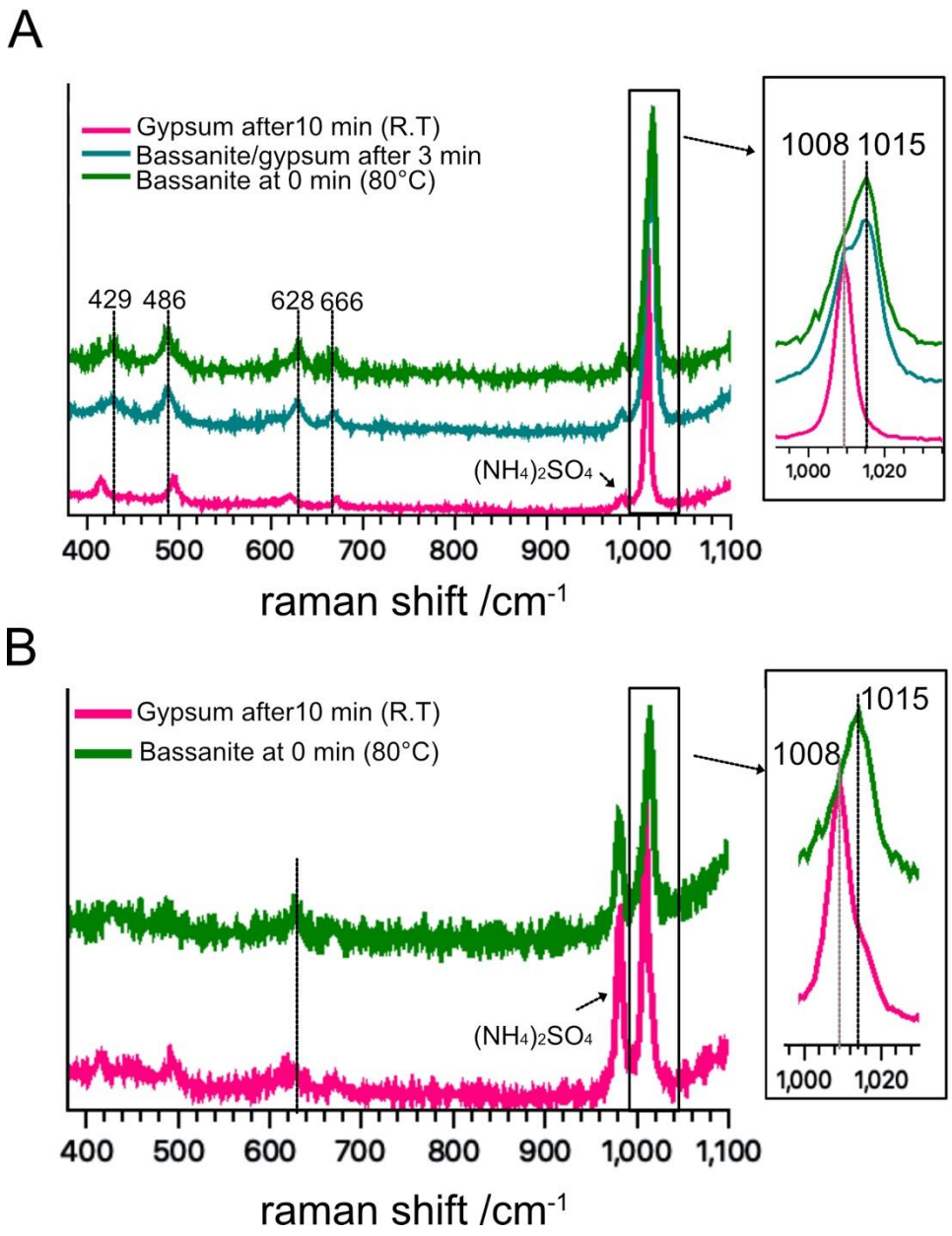

Figure S6. Raman spectra of the crystals precipitated at 80 **º**C by mixing equal volumes of (a) 300 mM $CaCl_2$ and 300 mM $(NH_4)_2SO_4$ solutions prepared by dissolving the solids in 5M $(NH_4)_2Cl$ aqueous solution, and (b) 3 M $CaCl_2$ and 3 M $(NH_4)_2SO_4$ aqueous solutions. The Raman spectra were recorded of 20 µl aliquots directly extracted from the reaction solution at different time points while cooling to room temperature over 10 min. In both solutions, bassanite alone was present at 0 min (80 ^oC), while gypsum was the sole phase after 10 min. Characteristic peaks of bassanite are 429 cm^{-1} and 487 cm^{-1} $v_2(SO_4)$,628 cm^{-1} and 666 cm^{-1}

$v_4(SO_4)$, and 1014 cm^{-1} $v_1(SO_4)$. Those from gypsum are 414 cm^{-1} and 493 cm^{-1} $v_2(SO_4)$, 619 cm^{-1} and 670 cm^{-1} $v_4(SO_4)$, and 1008 cm^{-1} $v_1(SO_4)$. The peak at 980 cm^{-1} derives from NH_4SO_4 due to its high background concentration.

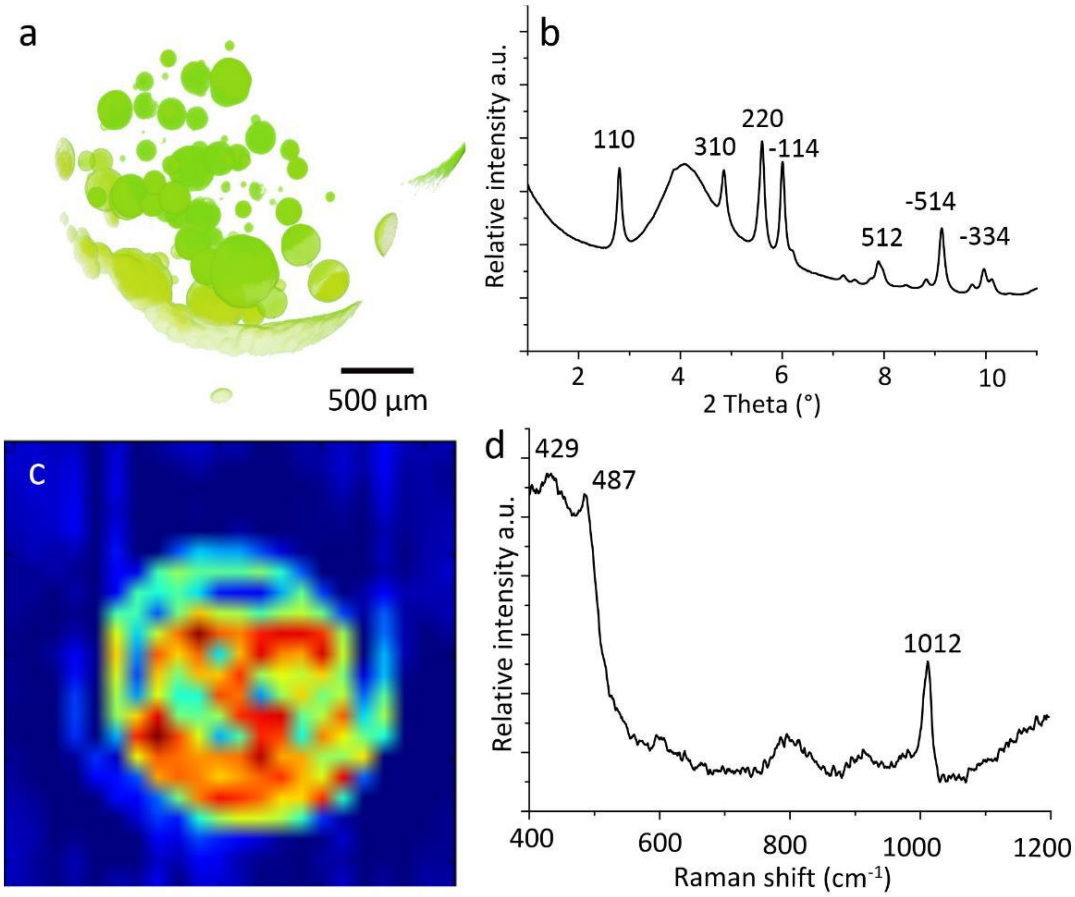

Figure S7. (a) 3D tomogram of bassanite crystals growing in a porous glass rod from 250 mM reagents after 18 h. (b) Diffraction pattern of the crystals in the pores and (c) 2D spatial diffraction map of the crystals after plotting the peak 110 with a 100 µm beam. (d) Raman spectra of bassanite crystals in the rod after 3 weeks from 250 mM solutions injection.

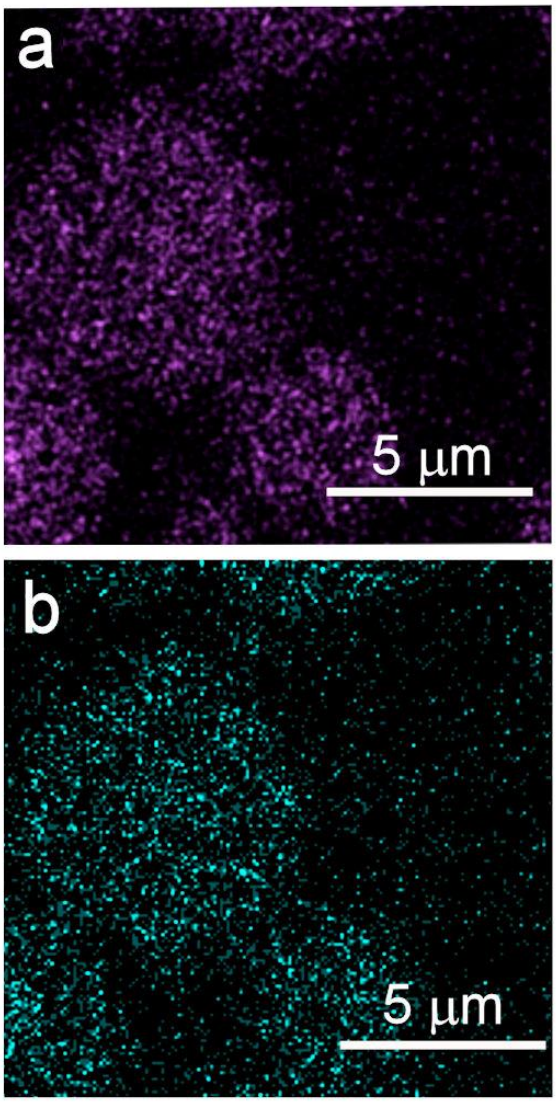

Figure S8. Energy dispersive x-ray (EDX) maps of a cross section through a CPG rod 7h after the outset of the experiment. Areas corresponding to the crystals are rich in (a) Ca and (b) S.

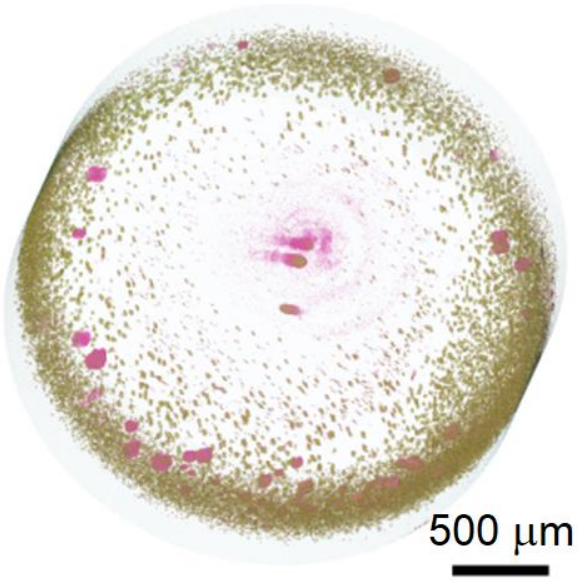

Figure S9. Rendered 3D μ-CT images of calcium sulphate crystals in a carboxyl-functionalised CPG rod after (A) 1h 15 min and (B) 1 h 30 min from $CaCl_2$ and 3M $(NH_4)_2SO_4$ solutions injection. The bassanite crystals are rendered green and the gypsum crystals pink. Scale bars are 500 μm.

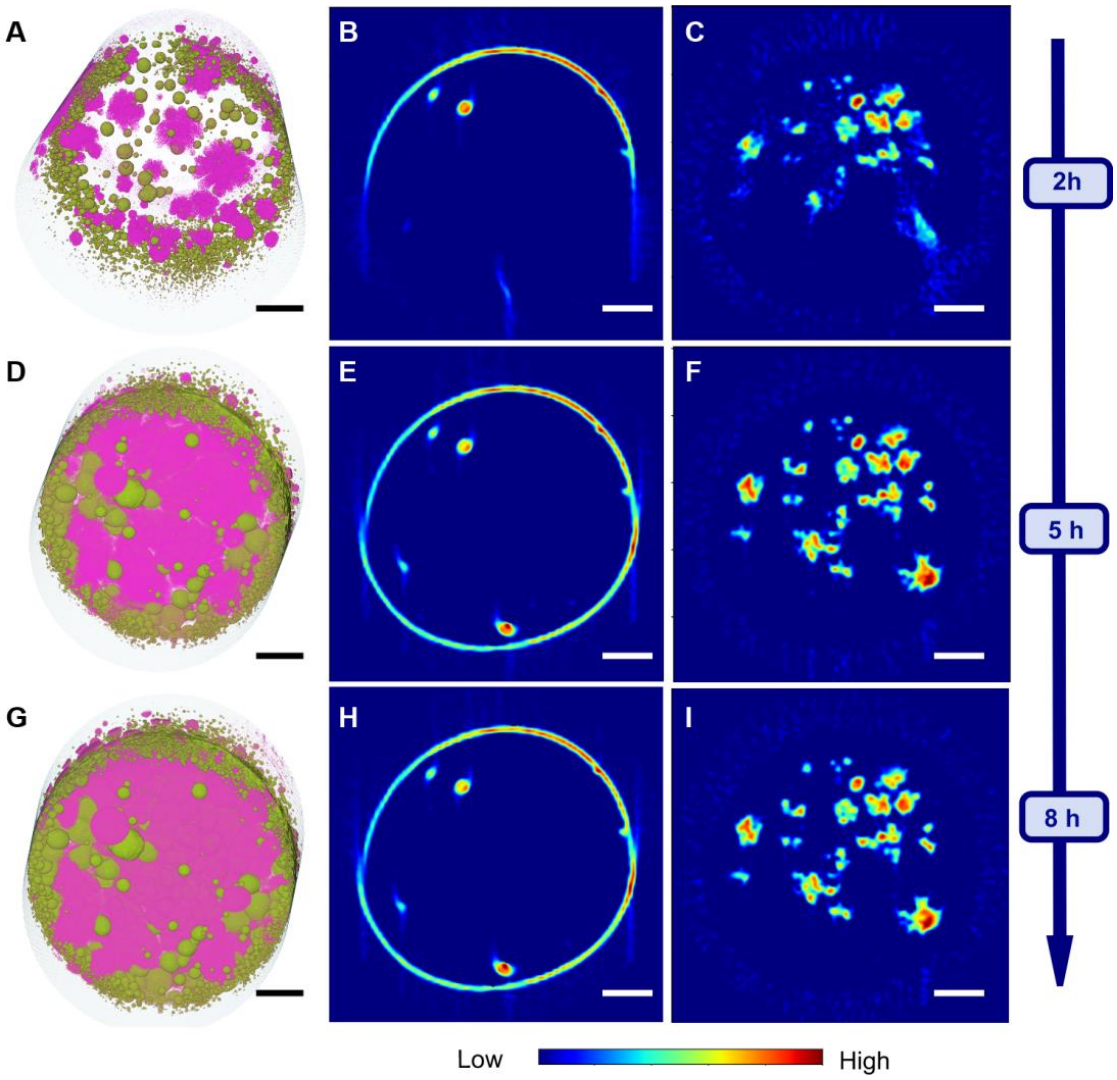

Figure S10. The evolution of calcium sulfate precipitation in carboxylate-functionalised CPG rod over time. (A, D, G) 3D µ-CT rendering of bassanite (green) and gypsum (pink) and (B, C, E, F, H, I) 2D X-ray diffraction computed tomography (XRDCT) maps of developing calcium sulfate crystals. The maps in (B, E, H) show circular bassanite crystals and were prepared using the (110) reflection from bassanite. A layer of bassanite is always found surrounding the rod. (C, F, I) show dendritic gypsum crystals, where these maps were created using the (020) reflection from gypsum. 5 h after reagent injection the rods become blocked and no further changes were observed by µ-CT or XRDCT. This is most clearly seen in 3D

images, where a given 2D slice may not be completely space filling. Note that different samples are shown in the μ-CT and XRDCT images. Scale bars are 500 μm.

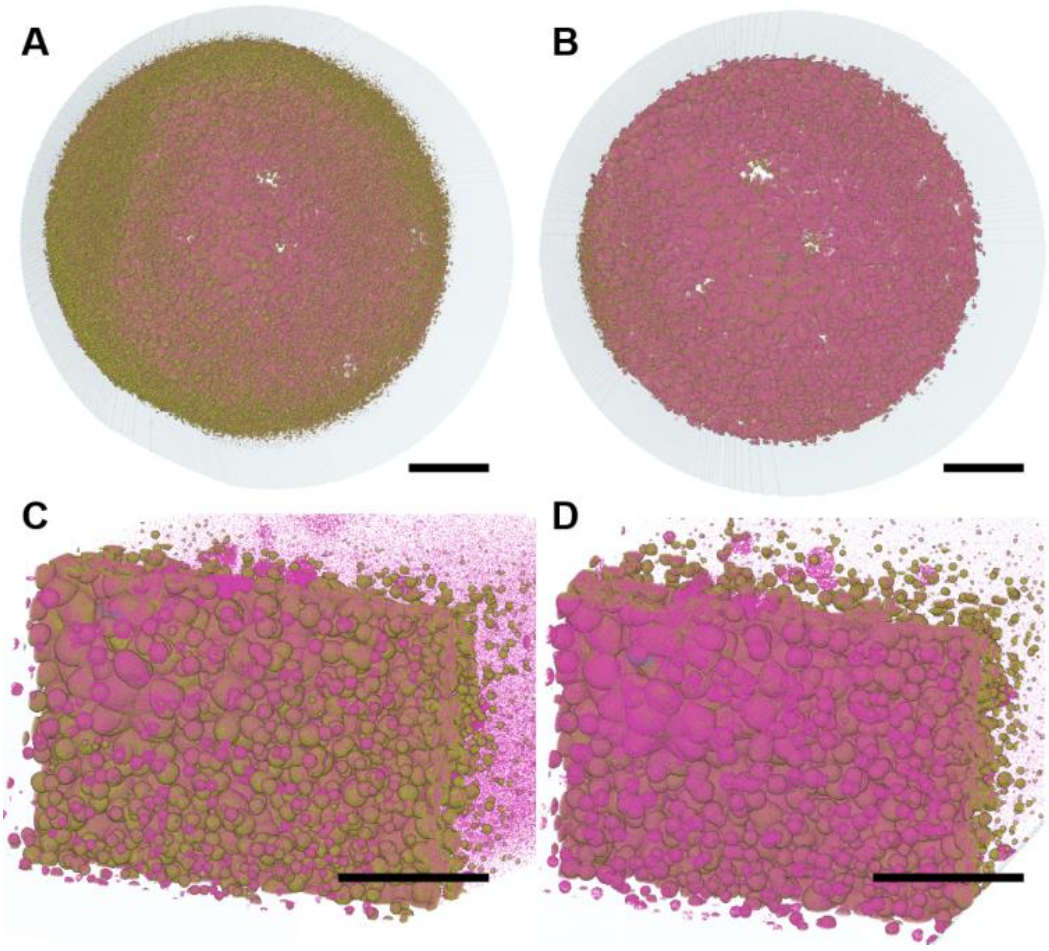

Figure S11. 3D rendering of μ-CT images of calcium sulfate crystals in a carboxyl-functionalized CPG rod after the reagents were replaced with water. (A and C) 5 h and (B and D) 8 h after water injection. The bassanite crystals are rendered green and the gypsum crystals pink. The pink specks seen in the background in (C) and (D) are due to background noise. Scale bars are 500 μm (A, B) and 250 μm (C, D).

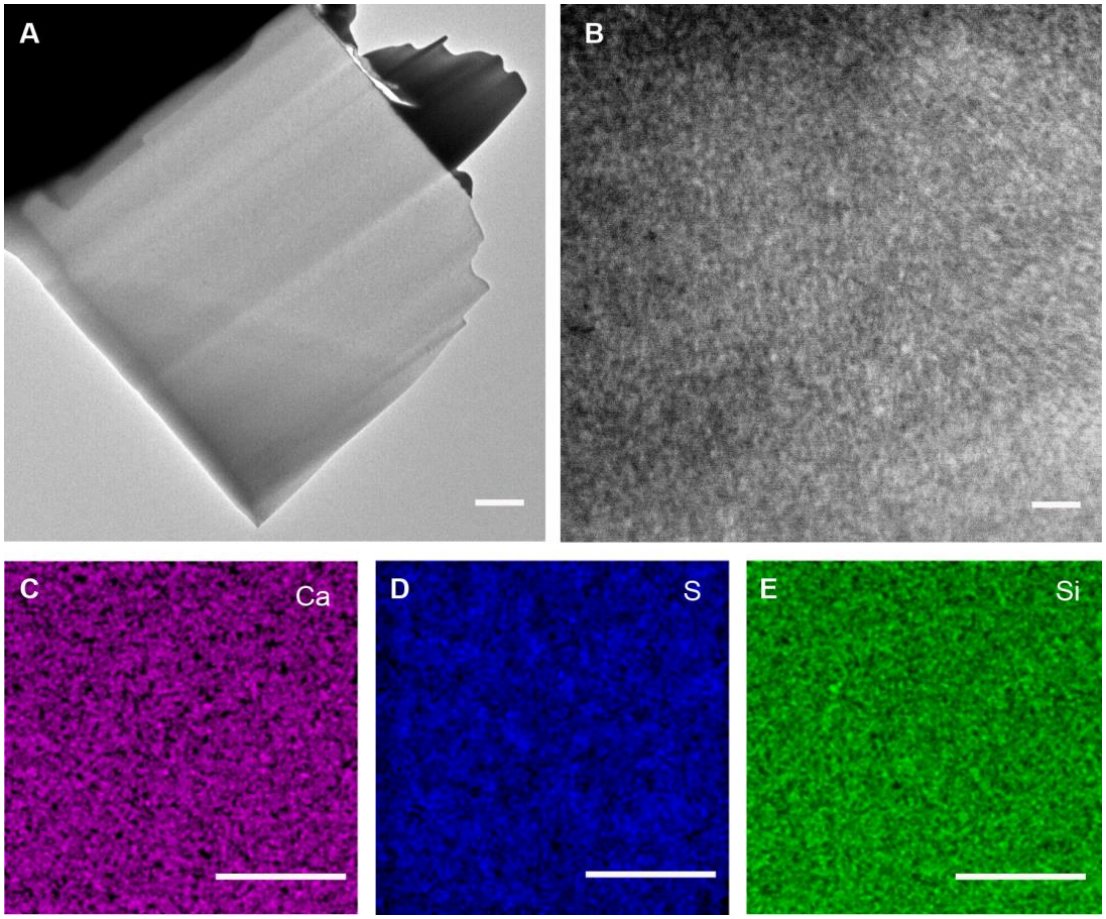

Figure S12. Analysis of CPG after transformation of bassanite to gypsum. (A and B) TEM images of a cross-section of a CPG rod containing calcium sulfate crystals as confirmed by STEM elemental mapping (C – E). Scale bars are 1 µm (A) and 100 nm (B-E).